PAPER

An encoded reconfigurable RFID strain sensor and its information fusion method

To cite this article: Lan Chen *et al* 2022 *Smart Mater. Struct.* **31** 105011

View the article online for updates and enhancements.

An encoded reconfigurable RFID strain sensor and its information fusion method

Lan Chen[1] , **Lei Kang**[1] , **Luyi Liu**[1], **Jingwen Hu**[2], **Guochun Wan**[2,*] and **Liyu Xie**[3]

[1] Department of Electrical and Electronic Engineering, Shanghai Institute of Technology, Shanghai, People's Republic of China
[2] Department of Electronic Science and Technology, Tongji University, Shanghai, People's Republic of China
[3] Department of Disaster Mitigation for Structures, Tongji University, Shanghai, People's Republic of China

E-mail: wanguochun@tongji.edu.cn

CrossMark

Abstract

Chip-based radio frequency identification (RFID) sensor systems have been investigated for structural health monitoring applications. However, the use of chips in sensor tags has drawbacks in terms of cost, durability, and detection capability. In this paper, we propose a reconfigurable RFID-based chipless tag sensor for strain detection, which detects structural strain by observing the offset of the resonant frequency of the antenna and incorporates an encoding unit for tag identification. To realize the reconfigurability of the antenna, a PIN diode is added to control the antenna, and the frequency reconfigurability of the antenna is realized by controlling the turn on/off of the PIN diodes. The Kalman filter algorithm is used to realize the information fusion of multiple sensors to improve the sensor detection accuracy, and the background noise data enhancement is used to expand the original data samples to fuse the information of the three sensors' data, and the relative error after fusion is reduced by about 36% compared with the relative error before fusion compared with separate measurements. The antenna was fabricated by an etching process and measured using vector network analyzer to verify the accuracy of the antenna simulation results.

Keywords: chipless RFID, strain sensors, reconfigurable, Kalman filtering, information fusion

(Some figures may appear in colour only in the online journal)

1. Introduction

To ensure that large bridges can serve reliably under the combined effects of environmental erosion, material aging, and catastrophic factors such as long-term effects of loading and fatigue effects, it is necessary to monitor the status of each bridge component in real-time and makes timely assessments of the bridge's health. With the development of modern detection and sensing technologies, wired sensor networks are deployed to monitor the health of building structures during construction. However, wired sensors require wiring and special parts of the wiring are difficult and vulnerable to environmental damage, and the length of the wiring will limit the transmission distance. Radio frequency identification (RFID) technology can realize distributed structural health monitoring (SHM) due to its advantages of low cost, passive wireless, and long reading distance. By processing and analyzing the data

---

collected by various sensors in real-time, the working status and health condition of the building structure can be understood on time.

RFID technology has been widely used in the field of SHM, especially the use of RFID antennas for characterizing strains [1–5], and cracks [6–8] on metals, and many results have been achieved.

Deck temperature is a parameter that is important to bridge operators. Bridge deck temperatures can approach 60 °C in summer, which is about 20 °C higher than the air temperature. High temperatures cause damage to the pavement, leading to rutting and permanent deformation [9], and Javed *et al* [10] proposed a multiparameter sensor for structural health inspection for detecting cracks and temperature changes in 2021. Since high temperatures also cause deformation of the bridge surface, it is also necessary to investigate the relationship between changes in these property parameters of the antenna and stress changes. The structural deformation caused by the structural stress change can be transferred to the antenna on the surface of the structure. Changing the dimensional parameters of the antenna changes the effective electrical length of the antenna surface, causing the resonant frequency to drift. Mc Gee *et al* [11] proposed a highly sensitive strain sensor and explored the effect of other factors on strain sensing in 2021; Li and Wang [12] proposed a strain and crack sensor with thermal stability for the SHM field that enables more reliable measurements in 2020.

Currently, wireless systems are evolving towards multifunctionality for fast, secure, and reliable communication, and antennas are one of the key enabling components that play a critical role in determining the ultimate performance of wireless systems. Traditional antennas are characterized by being fixed for specific functions, which severely limits the level of intelligence that can be introduced into multifunctional wireless systems. Therefore, many scholars have made exploratory attempts to control the intelligent aspects of RFID tags, and reconfigurable antennas provide sufficient flexibility and adaptability for the rapidly changing needs of wireless systems and their operating environments. An antenna pattern reconfiguration by controlling PIN diodes was proposed by Strangfeld *et al* [13] and Salas *et al* [14] proposed a frequency reconfigurable antenna was proposed by the length of liquid metal in 2018.

Chipless RFID sensors have great advantages in terms of cost, simplicity, printability, and the ability to work in high-temperature environments [14–17]. Therefore, the expansion of chipless RFID sensors in the field of SHM is of great interest.

Combined with the above research, the authors developed a coded reconfigurable RFID strain sensor based on the sensor being placed in the stress concentration, detecting the deformation of the measured structure by the offset of the resonant frequency, and adding PIN diodes to the coding unit to achieve reconfigurability and optimize the information, which also provides a new concept for the research of intelligent information processing technology. Among them, there have been basic research results in ID signal and sensing signal

detection, which can well support the research on multi-sensor information fusion.

2. Design and simulation verification of reconfigurable chipless RFID sensors

In this paper, a passive chipless reconfigurable RFID sensor with 4-bit tag encoding is proposed for SHM applications. The coding unit and the sensor are designed in different frequency bands by changing the structure and dimensions of the sensor. The antenna is subjected to lateral or longitudinal stretching, and a small change in size can change the resonant frequency of the antenna. We can observe the change of resonant frequency when strain is applied to the antenna, and then get the relationship between strain and resonant frequency change. This multi-sensor is designed using HFSS, as shown in figure 1.

The designed chipless tag consists of four half-electric-LC (ELC) resonators [18] and a split ring resonators (SRRs) resonator. RogersRT/Duroid5880 is used as the substrate and copper is used as the conducting heat sink. A PIN diode is added to the half-ELC resonator, and the 0–1 control of the code is achieved by controlling the turn on/off of the diode thus the path and effective electrical length of the antenna surface current are changed.

2.1. Construction of chipless RFID tag sensors

The proposed sensor tag consists of two resonator sections: the sensor section and the ID section. The sensor part of the tag is a SRR, while the ID part consists of four half-ELC resonators located on the left side of the SRR. These half-ELC resonators will generate a binary ID '1111' as the tag's code for tag identification.

The use of half-ELC is designed and optimized according to the ELC resonator. As shown in figure 2 to observe the results of HFSS simulation, if we choose the design of an ELC resonator coupled with a microstrip line, the value of return loss is greater than −10 dB, in the later stage of physical production and experimental testing, likely, the trapped wave cannot be detected. And the size of the ELC resonator is large, which is not conducive to the miniaturization of the antenna tag. To improve the performance of the antenna, a combination of coupling and connection is used.

Figure 3 shows the tag design using SRR and half-ELC resonators. In the tag design, W and L denote the width and length of the substrate, wi and li denote the width and length of the resonator, ei denotes the width of the internal slot of the resonator, a denotes the average length of the rectangular SRR, and dL denotes the gap length between consecutive resonators. The specifications and dimensions of all parameters are shown in table 1.

Two SRRs can be considered as a resonant pair and each resonant pair can be represented as an LC circuit that resonates at a specific resonant frequency [19]. The current flows along the microstrip line into the external SRR, an electric potential
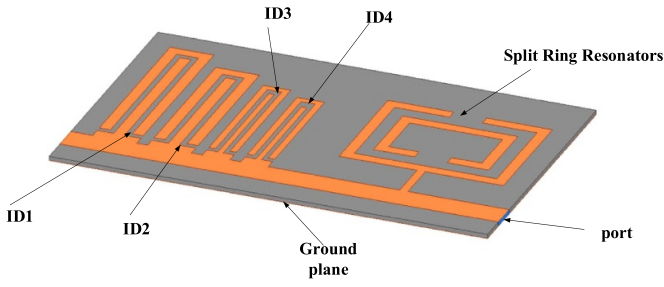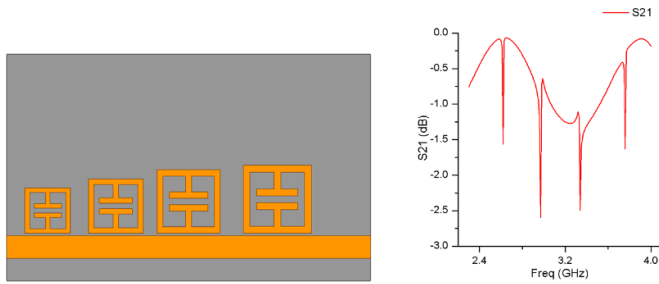
Figure 1. Chipless RFID tag.

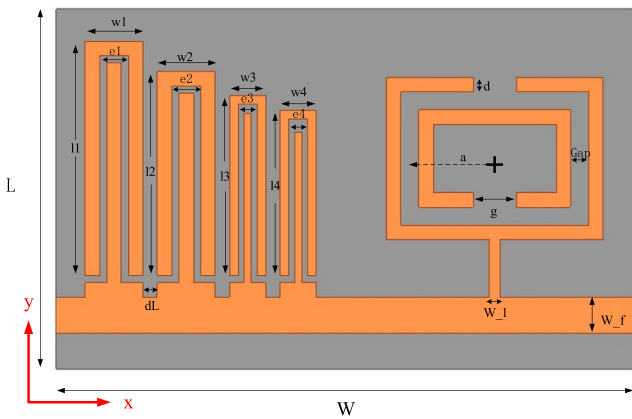**Figure 2.** ELC resonator coding label and its S21 result.

Figure 3. Dimensions of chipless RFID tag.

Table 1. Chipless RFID tag size (unit: mm).

	Value			
i	1	2	3	4
Li	32.5	28.3	25	22.9
wi	8	8	5	5
Ei	4	4	2.6	2.6
dL		2		
A		10.75		
ws		6		
D		2		
Gap		2.5		
W_l		1.5		
W_f		5		
W		50		
L		80		

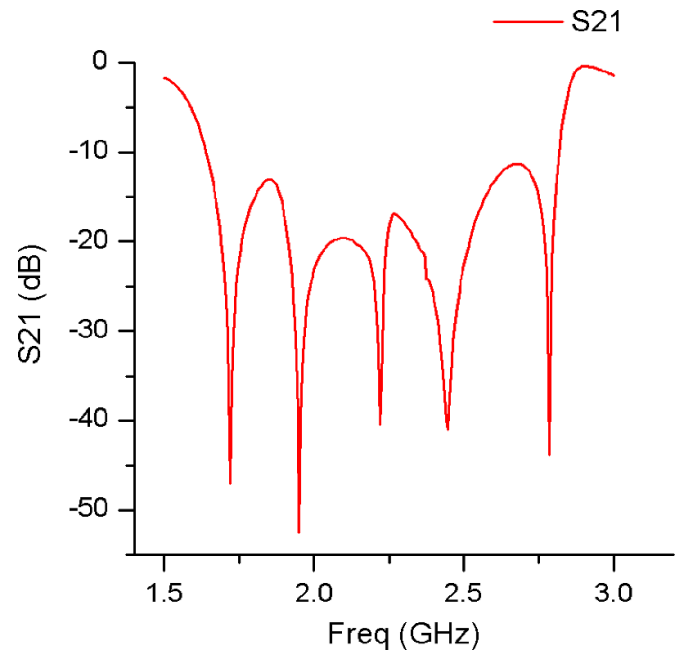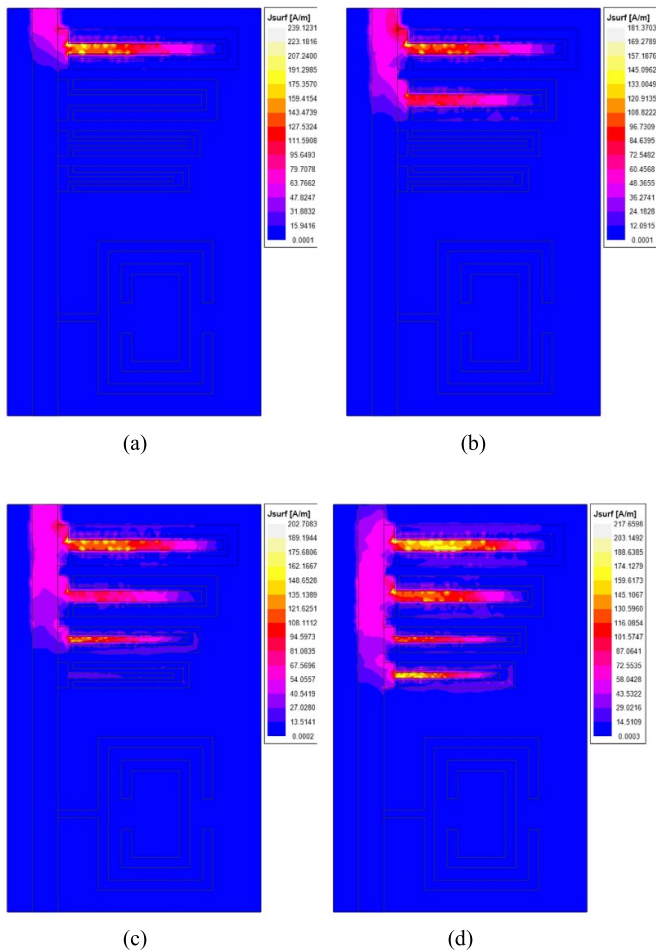*i*: Numbering of the four half-ELC resonators.

Figure 4. S21 result for chipless RFID sensor.

2.2. Model analysis and simulation

To further investigate the radiation characteristics of the sensor. We choose the Ansoft HFSS software for simulation, and the result of S21 is shown in figure 4. The substrate of the antenna tag is set to RogersRT/Duroid5880, and the copper sheet is attached to the substrate. Five resonant frequencies are generated in the frequency range. The first four resonant frequencies are generated by four half-ELC resonators at 1.72 GHz, 1.97 GHz, 2.22 GHz, and 2.46 GHz, and the last resonant frequency is generated by the SRR resonator at 2.80 GHz. By adjusting the size of the antenna, the resonant frequencies of the five units are separated without interfering with each other. The resonant frequency ID is defined as 1 and the non-resonant frequency is 0. The tag ID information is '1111'. For a 4-bit chipless RFID tag, the maximum amount

will appear around it and a current will be induced, which will pass from one ring to the other through the gap, and the resonant frequency is calculated by the following equation [20]:

$$
\begin{cases}
f = \dfrac{1}{2\pi\sqrt{L_{eq}C_{eq}}} = \dfrac{1}{2\pi\sqrt{L_{eq}\left[\left(2a-\frac{g}{2}\right)C_{pul}+\frac{\varepsilon_e ch}{2g}\right]}} \\[2mm]
C_{pul} = \dfrac{\sqrt{\varepsilon_e}}{C_0 Z_0} \\[2mm]
L_{eq} = 0.00508l\left(2.303 lg\frac{4l}{d}-\theta\right)
\end{cases}
\tag{1}
$$

where $C_0 = 3\times 10^8$ m s^{-1} is the speed of light in free space. ε_e is the effective dielectric constant of the medium and Z_0 is the impedance of the medium. l is the length and d is the width of the wire. The constant θ varies with the geometry of the wire.
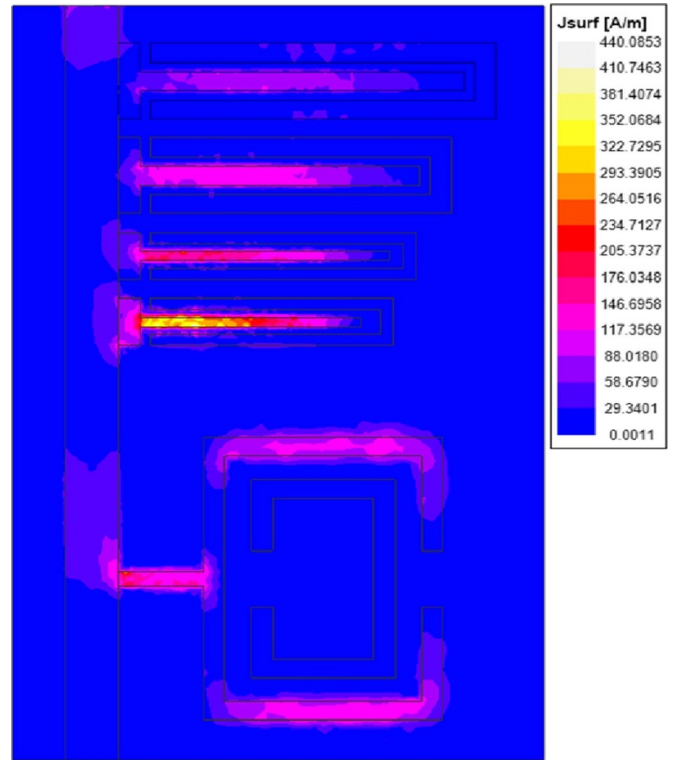
(a)

(b)

(c)

(d)

Figure 5. The current distribution of strain sensors with different resonant frequencies. (a) 1.72 GHz, (b) 1.97 GHz, (c) 2.22 GHz, (d) 2.46 GHz.

Figure 6. Current distribution at 2.80 GHz resonant frequency.

of information carried is $2^4 = 16$. The amount of information can be increased by increasing the resonant structure, but in the same frequency range, there may be false codes, making the antenna less reliable.

The resonant characteristics of the antenna tag are further understood by observing the surface current distribution of the radiating patch at the resonant frequency. As shown in figure 5, the coding unit of the 4-bit RFID sensor is designed with a half-ELC resonator to carry the information of 1111. As can be seen from the current distribution diagram, the resonant frequency increases as the resonator electrical length decrease for RFID tags ID1 to ID4. The current density at the end of the resonator short route and the peripheral U-shaped resonator is extremely small, so the resonator mainly relies on the coupling in the middle position to affect the resonant frequency.

The current distribution of the strain cell is shown in figure 6. By observing the current distribution of the SRR, it can be observed that the current of SRR is denser in the longitudinal direction, so when the RFID strain sensor undergoes deformation in different directions, the strain cell is affected differently and the resonant frequency changes in different patterns. When the longitudinal strain is applied, the

resonant frequency is more affected and the strain sensor is more sensitive.

2.2.1. Reconfigurable simulation. The frequency reconfigurable antenna can change the frequency by changing the electrical parameters while keeping the other characteristics of the antenna unchanged. By adding a PIN diode to the antenna surface, the resonant frequency of the tag can be changed by controlling the turn-on or turn-off of the PIN diode to change the path and effective electrical length of the current on the antenna surface.

The PIN diode is modeled using HFSS by setting the lumped *RLC* boundary of the PIN diode model to operate in different states. The equivalent circuits of the PIN diode in the on and off states are shown in figure 7 [21], respectively. In the on state, the PIN diode is modeled as a 1 Ω resistor in series with a 0.6 nH inductor, and in the off-state In the off state, the diode is modeled as a 0.5 pF capacitor and a 20 KΩ resistor in parallel and series with a 0.6 nH inductor. Two 1 μF capacitors are placed at each end of the PIN diode to provide the RF connection and block the DC. Through simulation, the position of two PIN diodes needs to be adjusted to make the best performance of the antenna simulation, the final PIN diode position as shown in figure 7, by controlling the PIN diode on or off to control the ID3, ID4 information and does not affect the rest of the ID information and sensor area information.

According to the S21 curve in figure 8, when PIN diodes 3 and 4 are both on, the coded information is 1111 when PIN diode 3 is off, the coded information is 1101 when PIN diode
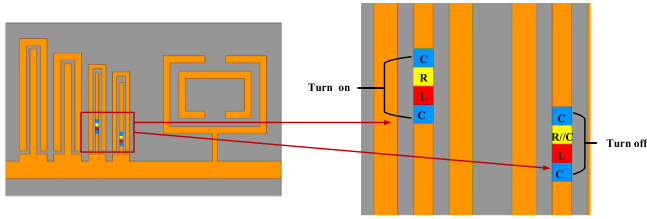
Figure 7. PIN diode on-model and off-model.
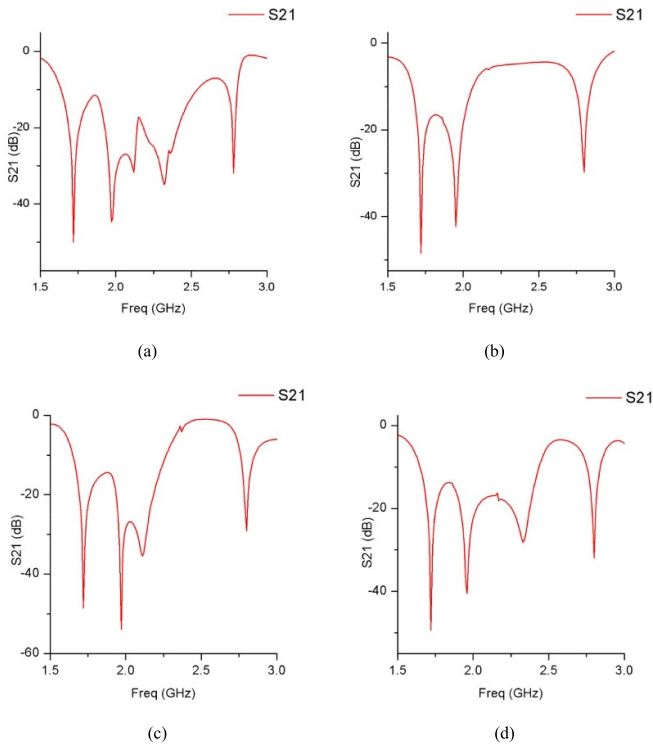
Figure 8. Different results of PIN diode turn on and turn off under different conditions. (a) 1111, (b) 1100, (c) 1110, (d) 1101.

4 is off, the coded information is 1110, and when both are off, the coded information is 1100.

2.3. Strain simulation

We choose the optimetrics function of Ansoft HFSS for strain simulation of the antenna to simulate the measurement of the transverse and longitudinal strain of the sensor. We assume here that the longitudinal strain of the patch antenna increases and the length of the antenna in the *y*-direction changes, thus leading to a change in the resonant frequency of the antenna. Assuming that the initial length of the antenna is l_0, a strain k occurs in the longitudinal direction and the longitudinal length of the antenna becomes l_y after the strain. Therefore,

$$k = \frac{l_y - l_0}{l_0}. \tag{2}$$

From equation (1):

$$f = \frac{c_0}{2\sqrt{\varepsilon_e}\,(l_0 + 2\Delta l)}. \tag{3}$$

(a)

(b)

(c)
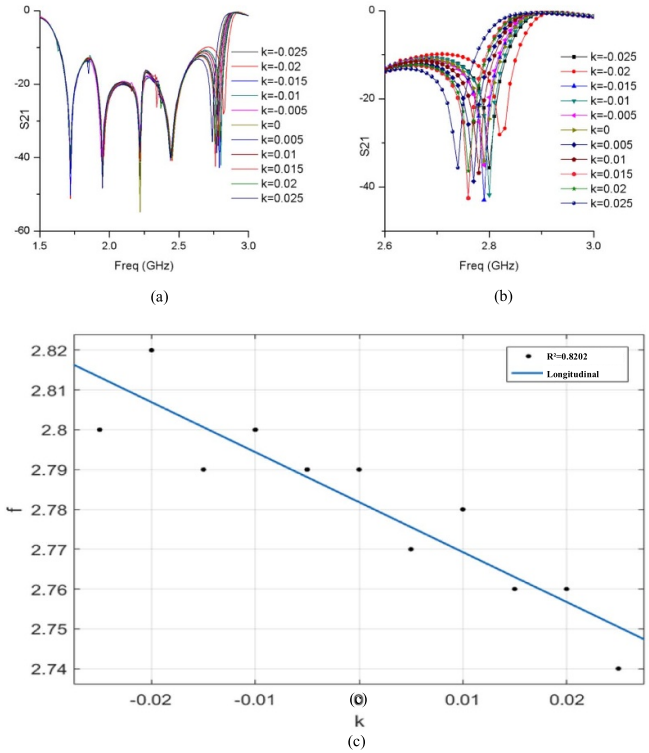
Figure 9. Frequency shift results and linear fit results for longitudinal strain. (a) Longitudinal strain results, (b) resonant frequency shift of the strain relief unit, (c) MATLAB linear fitting results.

Get further equation (4):

$$\begin{cases} f = \frac{c_0}{2\sqrt{\varepsilon_e}\,(l_0 + 2\Delta l)} = \frac{c_1}{l_0 + c_2 h} \\[2mm] c_1 = \frac{c}{2\sqrt{\varepsilon_e}} \\[2mm] c_2 = 0.824 \frac{(\varepsilon_e + 0.3)\left(\frac{w_0}{h_0} + 0.264\right)}{(\varepsilon_e - 0.258)\left(\frac{w_0}{h_0} + 0.813\right)} \end{cases}. \tag{4}$$

Considering the existence of the Poisson effect, the thickness of the dielectric substrate and the width of the radiating patch will change when the antenna is stretched longitudinally

$$\begin{cases} w_y = (1 - v_1 * k)\,w_0 \\ h_y = (1 - v_2 * k)\,h_0 \end{cases}. \tag{5}$$

v_1 refers to the Poisson's ratio of the length and width of the radiating patch. v_2 refers to the Poisson's ratio of the length of the radiating patch and the thickness of the dielectric substrate. From Wan *et al* [22] the final equation is simplified as:

$$f = f_0\,(1 - k). \tag{6}$$

Therefore, it can be assumed that in general when the rectangular microstrip patch antenna undergoes strain, its resonant frequency will produce an approximately linear shift.

The Poisson's ratio of copper material is set to 0.3, and the simulation results are shown in figure 9 with a change of k in steps of 0.005.
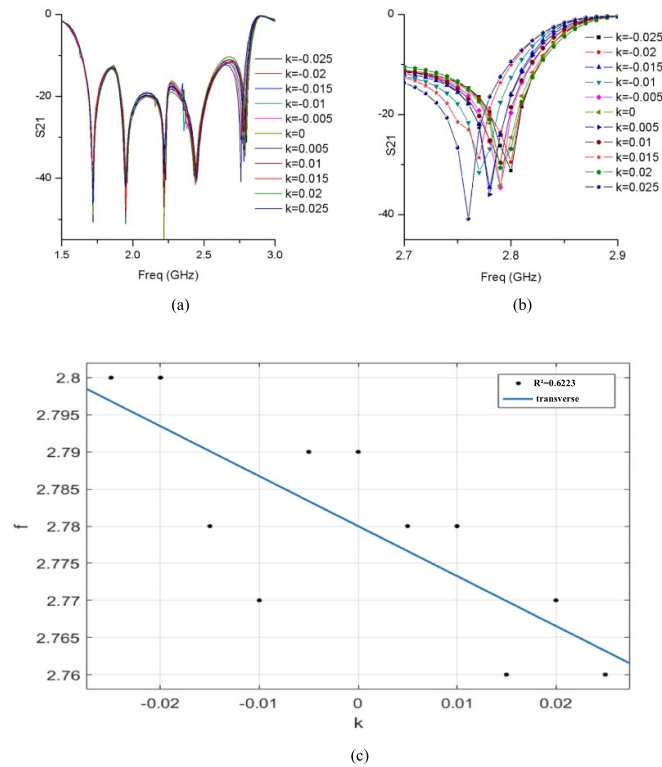
Figure 10. Frequency shift results and linear fit results for transverse strain. (a) Transverse strain results, (b) resonant frequency shift of the strain relief unit, (c) MATLAB linear fitting results.

As can be seen from figure 9, the resonant frequency of the rectangular strain sensor decreases as the degree of strain increases, while the resonant frequency of the encoded part remains unchanged. MATLAB was used to fit the scatter plot of resonant frequency to show that the change law between the resonant frequency of the rectangular patch and the strain is approximately linear, and the fitted linear equation is $y = -1.255x + 2.782$. The fitting result is shown in figure 9(c), for every 1 mm stretch, the resonant frequency changes by 25.1 MHz, and the magnitude of the coefficient of determination is 0.8202, which is good linearity.

Similarly, it can be seen that when the antenna undergoes transverse strain, the length of the antenna in the *x*-direction changes. The fitted linear equation is $y = -0.6727x + 2.78$. The fitting result is shown in figure 10(c), for every 1 mm stretch, the resonant frequency changes by 13.5 MHz, and the magnitude of the coefficient of determination is 0.6223, which has some linearity.

2.4. Broadband antennas for transmission and reception

To ensure that the antenna can work properly, it is also necessary to design a broadband antenna for signal transmission and reception. For the wideband antenna, the return loss is generally used to measure the matching degree of transmission line and antenna port, when the return loss is less than -10 dB, it indicates that the antenna is well-matched, and its corresponding frequency range is the bandwidth of the antenna.

The broadband antenna proposed in this paper for transmitting and receiving is a circular monopole, including a disk and
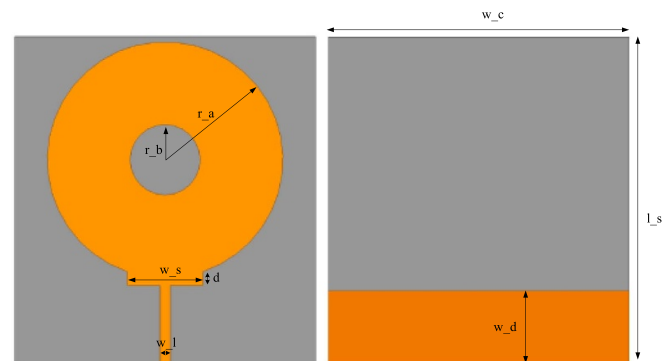

Figure 11. The front view and back view of the broadband antenna.

microstrip line in front and a grounding plate at the back, as shown in figure 11. The frequency range of the antenna can be varied by changing the radius of the disk and the width of the grounding plate. The rectangular parasitic patch is added under the circle to form a certain transition between the radiation patch and the feed line to improve the impedance matching. The final dimensions of the broadband antenna are shown in table 2.

Since the designed chipless RFID tag has an operating band of 1.7–2.8 GHz, the antenna parameters need to be set according to this operating frequency range. After an optimized design by simulation, the dimensions of the circular monopole antenna are determined as shown in table 2, and the return loss of the input port is shown in figure 12.

Table 2. The broadband antenna size (unit: mm).

Parameter	Value
r_a	23.5
r_b	7
w_s	15
D	2.728
w_l	2
w_d	14.5
W_c	60
L_c	65
H	0.785
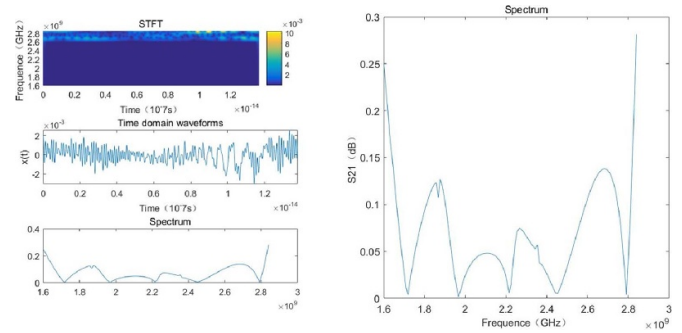
Figure 13. Results for tag sensor STFT.
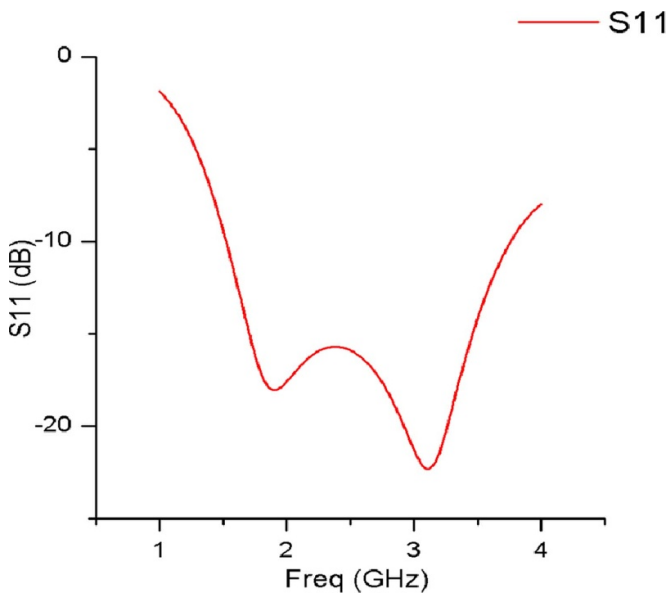
Figure 12. Broadband antenna simulation S11 curve.
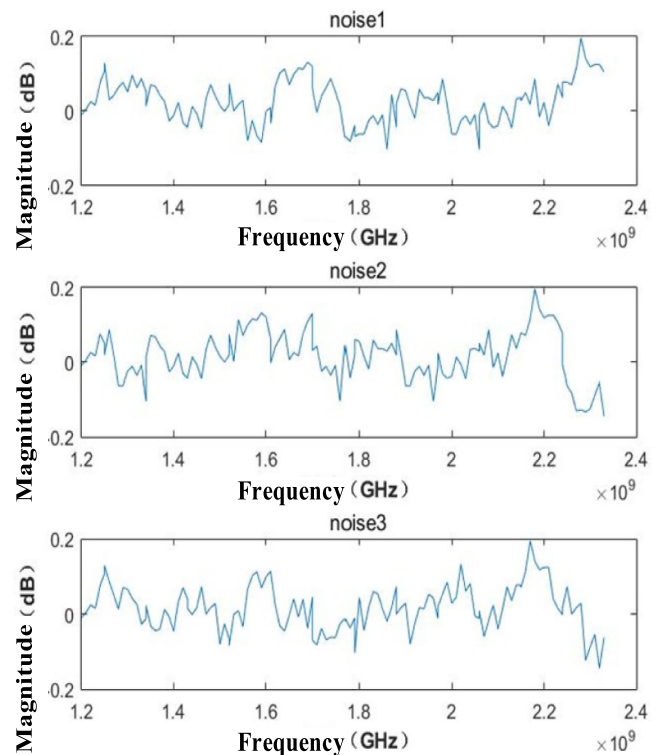

Figure 14. Acquired noise images.

3. Kalman filter-based multi-sensor information fusion

Estimation of the state of a target is one of the main purposes of multi-sensor data fusion. In the case of multiple targets, to complete the estimation of the target state it is necessary to accurately track the target, but the data measured by all sensors are interfered with by noise, which cannot be eliminated but only minimized, and the presence of noise often leads to the observed data not being able to accurately estimate the true state of the target, so filtering of the data is especially critical. The Kalman filtering algorithm can compensate for dynamic measurement errors and computational errors and can perform best estimates as well as perform recursive calculations, thus improving the accuracy of the measurement results.

3.1. Data preprocessing based on short time Fourier transform

The resonance frequency magnitude of the tag is determined by detecting the location of the appearance of spikes in the spectrum when the temporal metal radiator on the surface of the electromagnetic wave tag generates resonance. By using the short-time Fourier transform, the time-frequency spectrum

of the sensor tag can be obtained, and then the resonant peaks representing the ID and strain sensing regions of the sensor tag can be extracted [23]. As shown in figure 13, the characteristic distribution of specific tag and strain sensing regions can be seen on the short time fourier transform (STFT) spectrum.

3.2. Expansion of the original data sample

Due to the high practical cost of conducting multi-sensor fusion experiments, the background noise data enhancement is used to expand the original data samples, assuming that three sensors are used for fusion. The actual noise in the vector network analyzer (VNA) was collected as background noise enhancement, and the collected noise was added to the original data sample added noise signal as shown in figure 14. The frequency-domain information is first converted to time-domain information by STFT, and the time domain
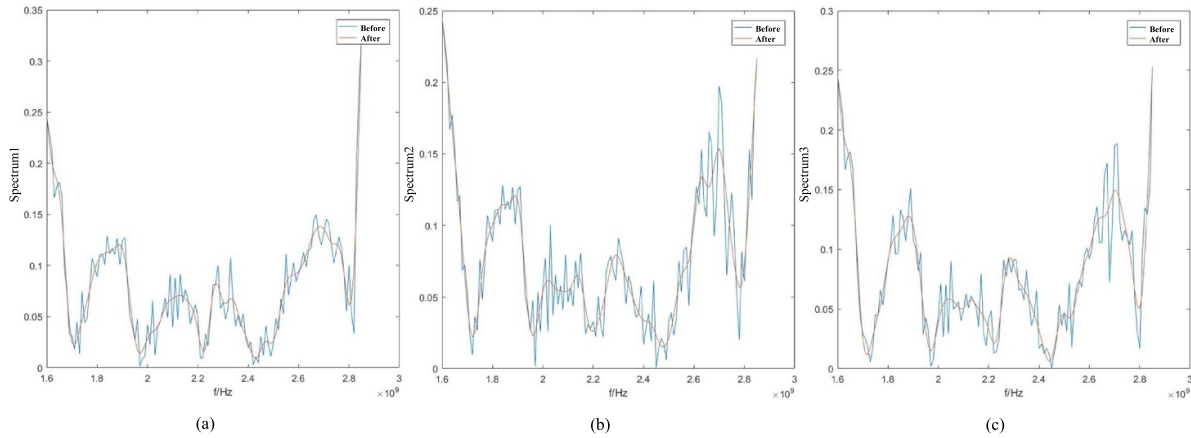
Figure 15. Sensor signal after smoothing processing. (a) Sensor 1, (b) sensor 2, (c) sensor 3.
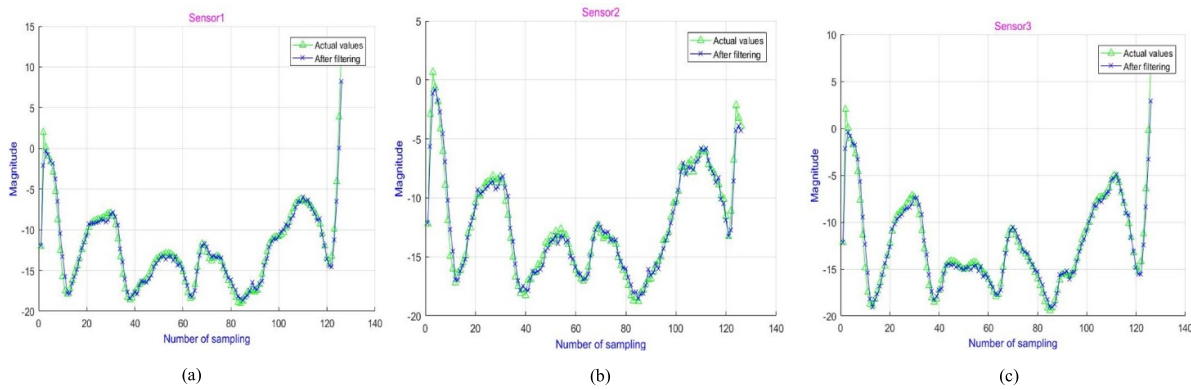

Figure 16. Sensor signal after smoothing processing. (a) Sensor 1, (b) sensor 2, (c) sensor 3.

signal is intercepted at a specific response time to obtain useful information, and then the time domain information is converted to frequency domain information by fast fourier transform (FFT), and the frequency domain information needs to be smoothed due to the addition of noise. A Butterworth filter is used to achieve smooth denoising, and here a low-pass filter is chosen to retain the signal within 0–0.15. The final three sensor signals obtained are shown in figure 15.

3.3. Multi-sensor information fusion

Due to the presence of device processes or other factors that cannot be controlled and noise, the prediction of physical quantities by sensors cannot be completely accurate. Therefore, the sensor measurements are considered as a random variable *v*, whose mean and variance are μ, $\sigma 2$, and multiple identical sensors are used to measure a physical quantity at the same time, and then summed or weighted average sums are obtained according to the reliability to reduce the effect of uncertainty. The results of the three sensors after Kalman filtering are shown in figure 16, and the three are fused and the results are shown in figure 17. The relative errors before and after fusion are calculated separately from
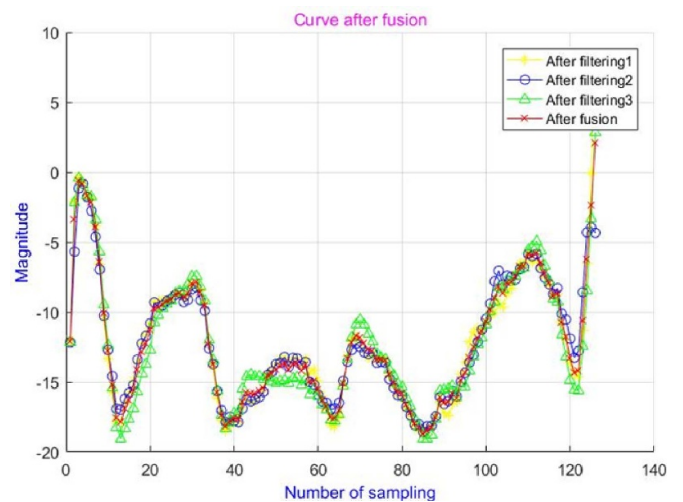
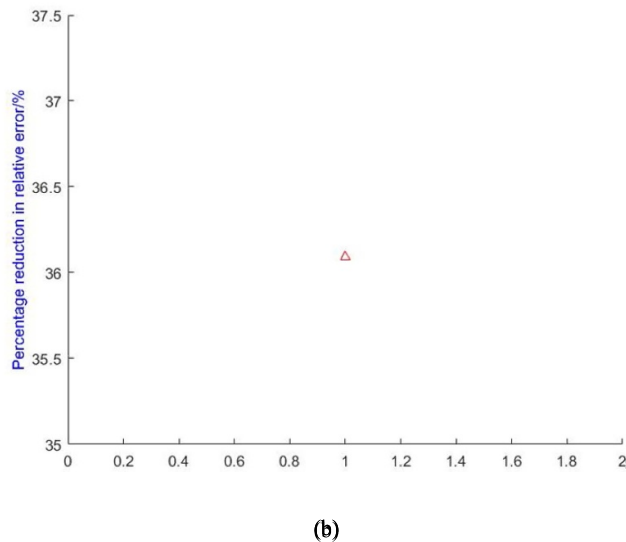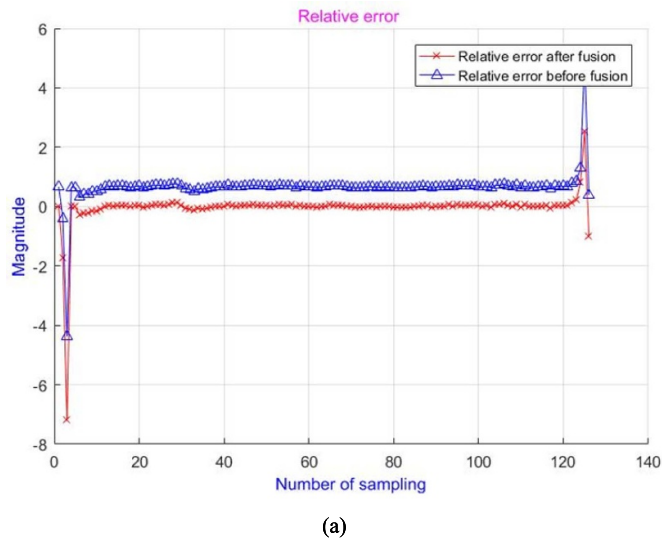

Figure 17. Results after sensor fusion.

the original data, as shown in figure 18. By comparing the average of the relative errors before and after fusion, it can be seen that the relative errors are reduced by about 36% after sensor fusion.

(a)

(b)

Figure 18. Comparison of relative error results before and after sensor fusion. (a) Comparison of relative error results before and after sensor fusion, (b) percentage of relative error reduction.

Figure 19. The antennas are made by the etching method. (a) Front view of the actual broadband antenna, (b) back view of the actual broadband antenna, (c) front view of the actual strain sensor, (d) back view of the actual strain sensor.

Figure 20. The process of physical measurement of antennas. (a) S21 results for physical measurements of strain sensors, (b) results of physical strain sensors measured with VNA, (c) wired measurement of strain, (d) wired measurement of strain sensors.
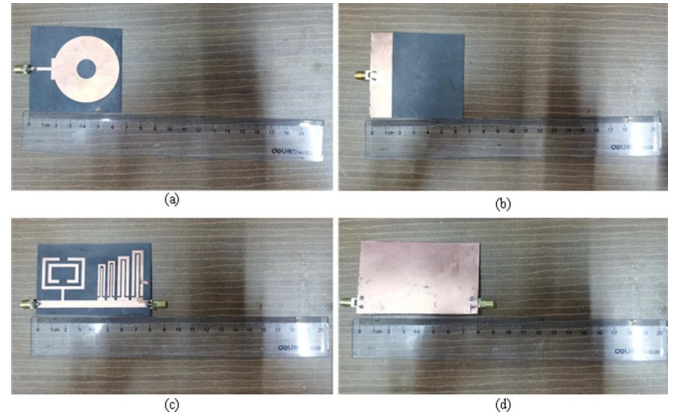
4. Fabrication and detection of chipless RFID sensors
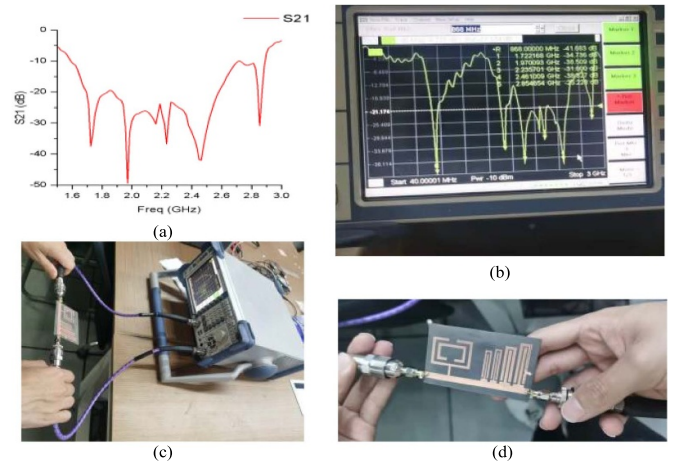
4.1. Chipless RFID strain sensor fabrication

The chipless RFID strain sensor and the broadband antenna for transmitting and receiving are fabricated using an etching process with a Rogers RT/Duroid5880 substrate, and the fabricated sensor is shown in figure 19. The broadband antenna in the figure has been soldered with a Sub-Miniature-A (SMA) adapter, and the fabricated antenna meets the simulation performance requirements.

4.2. Chipless RFID strain sensor detection experiment

Due to the existence of processing technology, testing environment, and instruments, the measured resonant frequency of the antenna under test and the simulation results will have

some differences, but this does not affect the actual experimental analysis and demonstration, because the object of study is not the resonant frequency itself, but the offset of the resonant frequency, the offset of the resonant frequency is a relative value rather than an absolute value, therefore, before the actual experiment, the actual resonant frequency of the antenna under test needs to be measured first. For the strain transducer with wired measurement, SMA adapters were soldered on both ends of the microstrip transmission line for connection to the VNA, while for the strain transducer with wireless measurement, no connection was needed, and the information was collected through a pair of broadband antennas. As shown in figure 20, the VNA shows from 40 MHz, the signal is valid from 1.5 GHz. The measurement results show that there are burrs at the third trap and a very small shift in frequency due to the processing process and test environment, but the overall results are good.

5. Conclusion

In this paper, a chipless RFID reconfigurable strain sensor was designed and fabricated under laboratory conditions. The current distribution analysis was used to investigate the strain magnitude and direction. A PIN diode was added to the coding unit, and frequency reconfigurability was achieved by controlling the turn-on or turn-off of the PIN diode. The data samples were extended by the method of background noise data enhancement, and multi-sensor fusion detection was achieved using the Kalman filtering algorithm to improve the detection accuracy. In the future, we can consider that we should improve the accuracy of wireless detection of RFID antennas and improve detection devices, such as using portable VNAs to achieve anytime, anywhere measurements and improve the performance of the sensors themselves through improved algorithms.

Data availability statement

All data that support the findings of this study are included within the article (and any supplementary files).

Acknowledgments

ORCID iDs

Lan Chen ● https://orcid.org/0000-0002-5747-7761
Lei Kang ● https://orcid.org/0000-0003-2207-5137
Guochun Wan ● https://orcid.org/0000-0003-0521-1176
Liyu Xie ● https://orcid.org/0000-0001-5777-0645

References

[1] Xiaohua Y, Cho C, Wang Y and Tentzeris M M 2016 Battery-free slotted patch antenna sensor for wireless strain and crack monitoring *Smart Struct. Syst.* **18** 1217–31
[2] Cho C, Yi X, Li D, Wang Y and Tentzeris M M 2016 Passive wireless frequency doubling antenna sensor for strain and crack sensing *IEEE Sens. J.* **16** 5725–33
[3] Chakaravarthi G, Logakannan K P, Philip J, Rengaswamy J, Ramachandran V and Arunachalam K 2018 Reusable passive wireless RFID sensor for strain measurement on metals *IEEE Sens. J.* **18** 5143–50
[4] Kuhn M F, Breier G P, Dias A R and Clarke T G 2018 A novel RFID-based strain sensor for wireless structural health monitoring *J. Nondestruct. Eval.* **37** 1–10
[5] Kuhn M F, Breier G P and Clarke T G 2018 Passive wireless sensor for displacement monitoring in metal structures *IEEE Lat. Am. Trans.* **16** 1353–7

[6] Zhang J and Tian G Y 2016 UHF RFID tag antenna-based sensing for corrosion detection and characterization using principal component analysis *IEEE Trans. Antennas Propag.* **64** 4405–14
[7] Salim A, Naqvi A H, Pham A D and Lim S 2020 Complementary split-ring resonator (CSRR)-loaded sensor array to detect multiple cracks: shapes, sizes, and positions on metallic surface *IEEE Access* **8** 151804–16
[8] Norouzi M, Masoumi N and Jahed H 2021 Nondestructive phase variation-based chipless sensing methodology for metal crack monitoring *IEEE Trans. Instrum. Meas.* **70** 1–11
[9] Niu Y, Wang Y E and Tang Y 2020 Analysis of temperature-induced deformation and stress distribution of long-span concrete truss combination arch bridge based on bridge health monitoring data and finite element simulation *Int. J. Distrib. Sens. Netw.* **16** 10
[10] Javed N, Azam M A and Amin Y 2021 Chipless RFID multisensor for temperature sensing and crack monitoring in an IoT environment *IEEE Sens. Lett.* **5** 1–4
[11] Mc Gee K, Anandarajah P and Collins D 2021 Proof of concept novel configurable chipless RFID strain sensor *Sensors* **21** 6224
[12] Li D and Wang Y 2020 Thermally stable wireless patch antenna sensor for strain and crack sensing *Sensors* **20** 3835
[13] Strangfeld C, Johann S and Bartholmai M 2019 Smart RFID sensors embedded in building structures for early damage detection and long-term monitoring *Sensors* **19** 5514
[14] Salas M, Hübner M, Borysov M, Koerdt M, Rennoch M, Herrmann A S and Lang W 2018 Measuring material moisture in fiber reinforced polymers by integrated sensors *IEEE Sens. J.* **18** 3836–43
[15] Preradovic S and Karmakar N C 2010 Chipless RFID: bar code of the future *IEEE Microw. Mag.* **11** 87–97
[16] Tedjini S, Karmakar N, Perret E, Vena A, Koswatta R and Rubayet E 2013 Hold the chips: chipless technology, an alternative technique for RFID *IEEE Microw. Mag.* **14** 56–65
[17] Karmaker N C 2016 Tag, you're it radar cross section of chipless RFID tags *IEEE Microw. Mag.* **17** 64–74
[18] Lee S, Kim U, Kwon K, Seo W and Choi J 2012 Design of on-body antenna for wireless body area network *2012 14th Int. Conf. on Advanced Communication Technology (ICACT)* pp 300–3
[19] Sai D M, Mishra D P and Behera S K 2021 Frequency shift coded chipless RFID tag design using square split ring resonators *2021 2nd Int. Conf. on Range Technology (ICORT)* pp 1–4
[20] Saha C and Siddiqui J Y 2011 A comparative analyis for split ring resonators of different geometrical shapes *2011 IEEE Applied Electromagnetics Conf. (AEMC)* pp 1–4
[21] Kumar J, Basu B and Talukdar F A 2019 Modeling of a PIN diode RF switch for reconfigurable antenna application *Sci. Iran.* **26** 1714–23
[22] Wan G C, Xue K, Gao R X, Lv J Y and Tong M S 2018 A rectangular microstrip patch antenna used for structural health monitoring *2018 IEEE Int. Symp. on Antennas and Propagation and USNC/URSI National Radio Science Meeting* pp 695–6
[23] Wan G, Li M, Zhang M, Kang L and Xie L 2022 A novel information fusion method of RFID strain sensor based on microstrip notch circuit *IEEE Trans. Instrum. Meas.* **71** 1–10